Inorganic Chemistry

ARTICLE

pubs.acs.org/IC

Crystal Water Molecules as Magnetic Tuners in Molecular Metamagnets Exhibiting Antiferro−Ferro−Paramagnetic Transitions

Radovan Herchel,*[,†] Jiří Tuček,[‡,§] Zdeněk Trávníček,[†,§] Dimitris Petridis,[∥] and Radek Zbořil*[,‡,§]

[†]Department of Inorganic Chemistry and [‡]Department of Physical Chemistry, Faculty of Science, Palacky University in Olomouc, 17 Listopadu 12, 771 46 Olomouc, Czech Republic

[§]Regional Centre of Advanced Technologies and Materials, Faculty of Science, Palacky University in Olomouc, Slechtitelu 11, 783 71 Olomouc, Czech Republic

[∥]Institute of Materials Science, NCSR "Demokritos", 153 10 Ag. Paraskevi Attikis, Athens, Greece

Supporting Information

ABSTRACT:

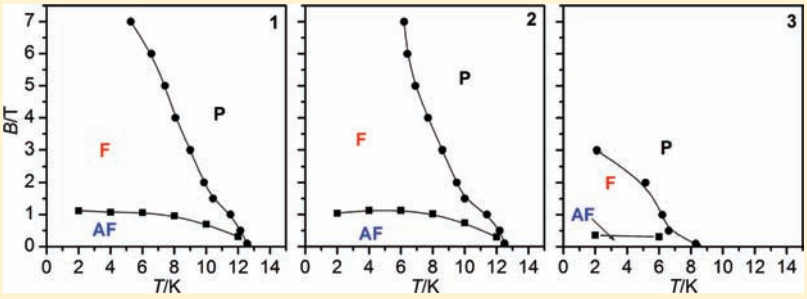

We studied the effects of the number of crystal water molecules on the magnetic behavior of $\{[Ni(en)_2]_3[Fe(CN)_6]_2 \cdot xH_2O\}_n$ (**1**−**3**) (where en = ethylenediamine and x = 3, 2, or 0) coordination polymers by ^{57}Fe Mössbauer spectroscopy, single-crystal X-ray diffraction, and magnetization measurements. Magnetic phase diagrams constructed for all three compounds indicate that they behave as metamagnets exhibiting very rare field-induced antiferro−ferro−paramagnetic transitions. The number of crystal water molecules has a major effect on the Néel temperature, critical field, and magnetic hardness of the compounds in the ferromagnetic state. Moreover, the systems behave as molecular magnetic sponges, changing their magnetic properties due to the controllable and reversible dehydration/hydration process.

INTRODUCTION

Magnetically ordered materials have attracted great interest since prehistoric times, and their uses have expanded in the last century due to rapid progress (inter alia) in computing and information storage.[1] Furthermore, demands from new technologies and the global miniaturization of electronic devices have induced rapid advances in coordination chemistry, leading to the discovery of a new class of magnetic materials called molecule-based magnets.[2,3] The most striking advantage of these compounds over conventional network-based, inorganic solid magnets is that their magnetic properties can be finely tuned by fine chemical modification of their composition and structure. In addition, the amount of crystal solvent molecules (e.g., water) present can significantly change their magnetic properties by shifting the critical temperature of their magnetic ordering or altering the nature of their magnetic phases. Such solvent-induced modulation of magnetic properties was first observed by Kahn et al., and the term "molecular magnetic sponge" was coined to describe cases in which the solvation−desolvation process is reversible.[4] This sensitivity to external stimuli can be employed in molecular sensors/switchers. Unfortunately, the range of potential applications of these species is usually limited by the low critical temperature of molecular magnets. However, the advent of coordination compounds featuring polycyanidometalate building blocks has led to the development of diverse new compounds with a variety of structural motifs and interesting magnetic properties,[5] including *room-temperature molecular magnets*.[6]

Of particular interest, in the context of this study, the hexacyanoferrate(III) anion $[Fe(CN)_6]^{3-}$ provides an efficient bridging ligand for preparing ferromagnets, ferrimagnets, and metamagnets.[7] Moreover, molecular compounds incorporating hexacyanoferrate exhibit various photomagnetic properties.[8] The coordination polymer $\{[Ni(en)_2]_3[Fe(CN)_6]_2 \cdot 2H_2O\}_n$ (en = ethylenediamine) was the first reported Ni(II)−Fe(III)$(CN)_6$ molecular magnet.[9] This compound was prepared by reacting $[Ni(en)_2Cl_2]$ and $K_3[Fe(CN)_6]$ in water and was identified as a ferromagnet with T_C = 18.6 K on the basis of zero-field-cooled and field-cooled magnetization measurements. However, it was subsequently reported that the same compound, prepared by the same synthetic procedure, acted as a metamagnet and that when prepared by reacting $[Ni(en)_3]X_2$ (X = Cl^- or ClO_4^-) and

Received: June 29, 2011
Published: August 24, 2011

Table 1. Bimetallic Cyanido-Bridged Molecular Magnets Based on Hexacyanoferrate(III) and Nickel(II) Complex Ions (for simplicity, the curly braces indicating the polymeric character of the complexes were omitted) in the Chronological Order in Which They Were Reported[a]

compound	type of magnetic ordering	critical parameters	structural motif	ref
$[Ni(en)_2]_3[Fe(CN)_6]_2 \cdot 2H_2O$	ferromagnet	T_C = 18.6 K	1D rope-ladder chain structure	9
$[Ni(pn)_2]_2[Fe(CN)_6]ClO_4 \cdot 2H_2O$	ferromagnet	T_C = 10 K	2D squares Fe_4Ni_4	22
$[Ni(tren)]_3[Fe(CN)_6]_2 \cdot 6H_2O$	ferrimagnet	T_C = 8 K	3D	23
$[Ni(pn)_2]_2[Fe(CN)_6]ClO_4 \cdot 2H_2O$	metamagnet	T_N = 8 K, B_c = 0.38 T (4.2 K)	2D	24
$[Ni(1,1\text{-dmen})_2]_2[Fe(CN)_6]ClO_4 \cdot 2H_2O$	metamagnet	T_N = 11.1 K, B_c = 0.18 T (4.2 K)	squares Fe_4Ni_4	
$[Ni(1,1\text{-dmen})_2]_2[Fe(CN)_6]BF_4 \cdot 3H_2O$	metamagnet	T_N = 14.6 K		
$[Ni(1,1\text{-dmen})_2]_2[Fe(CN)_6]PF_6 \cdot 2H_2O$	metamagnet	T_N = 11.0 K		
$[(Ni(bpm)_2)_3(Fe(CN)_6)_2] \cdot 7H_2O$	ferromagnet	T_C = 23 K	0D pentanuclear cluster	25
$[Ni(pn)_2]_2[Fe(CN)_6]ClO_4 \cdot 2H_2O$	metamagnet	T_N = 8 K, B_c = 0.38 T (4.2 K)	2D	26
$[Ni(pn)_2]_2[Fe(CN)_6]BF_4 \cdot 2H_2O$	metamagnet	T_N = 10.1 K	squares Fe_4Ni_4	
$[Ni(pn)_2]_2[Fe(CN)_6]PF_6 \cdot 2H_2O$	metamagnet	T_N = 9.4 K		
$[Ni(1,1\text{-dmen})_2]_2[Fe(CN)_6]ClO_4 \cdot 2H_2O$	metamagnet	T_N = 11.1 K, B_c = 0.18 T (4.2 K)		
$[Ni(1,1\text{-dmen})_2]_2[Fe(CN)_6]PF_6 \cdot 2H_2O$	metamagnet	T_N = 11.0 K		
$[Ni(1,1\text{-dmen})_2]_2[Fe(CN)_6]NCS \cdot H_2O$	metamagnet	T_N = 18.3 K		
$[Ni(1,1\text{-dmen})_2]_2[Fe(CN)_6]BF_4 \cdot 5H_2O$	ferromagnet	T_C = 14.6 K		
$[Ni(1,1\text{-dmen})_2]_2[Fe(CN)_6]CF_3SO_3 \cdot 2H_2O$	ferromagnet	T_C = 9.5 K		
$[Ni(1,1\text{-dmen})_2]_2[Fe(CN)_6]BzO \cdot 6H_2O$	ferromagnet	T_C = 9.3 K		
$[Ni(1,1\text{-dmen})_2]_2[Fe(CN)_6]I \cdot 4H_2O$	ferromagnet	T_C = 15.2 K		
$[Ni(1,1\text{-dmen})_2]_2[Fe(CN)_6]N_3 \cdot 4H_2O$	ferromagnet	T_C = 9.7 K		
$[Ni(1,1\text{-dmen})_2]_2[Fe(CN)_6]NO_3 \cdot 4H_2O$	ferromagnet	T_C = 16.2 K		
$[Ni(en)_2]_3[Fe(CN)_6]_2 \cdot 2H_2O$	metamagnet	T_N = 18.6 K	1D rope-ladder chain	10
$[Ni(L1)]_3[Fe(CN)_6]_2 \cdot 9H_2O$	metamagnet	T_N = 5 K, B_c = 0.1 T (1.93 K)	2D honeycomb-like Fe_6Ni_6	27
$[Ni(cyclam)]_3[Fe(CN)_6]_2 \cdot 22.5H_2O$	metamagnet	T_N = 8 K, B_c = 0.5 T (3 K)	2D	28
	canted-magnet	T < 3 K	honeycomb-like Fe_6Ni_6	
$[Ni(L2)]_3[Fe(CN)_6]_2 \cdot 12H_2O$	ferromagnet	T_C = 9.1 K, B_c = 0.15 T (1.6 K)	2D brick wall-like	29
$[Ni(tn)]_5[Fe(CN)_6]_3ClO_4 \cdot 2.5H_2O$	ferromagnet	T_C = 10 K, B_c = 0.04 T (5 K)	3D	30
$[Ni(L3)]_3[Fe(CN)_6]_2 \cdot 8H_2O$	metamagnet	T_N = 6 K, B_c = 0.09 T (1.93 K)	2D honeycomb-like Fe_6Ni_6	31
$[Ni(ampy)_2]_3[Fe(CN)_6]_2 \cdot 6H_2O$	ferromagnet	T_C = 7.5 K, B_c = 0.033 T (2 K)	undetermined	32
$[Ni(2,2'\text{-bipy})_2]_3[Fe(CN)_6]_2 \cdot 13H_2O$	ferromagnet	T_C = 11 K, B_c = 0.006 T (5 K)	0D pentanuclear cluster	33
$[Ni(cyclam)]_3[Fe(CN)_6]_2 \cdot 16H_2O$	metamagnet	T_N = 8 K	2D honeycomb-like Fe_6Ni_6	34
$[Ni(1,1\text{-dmen})_2]_2[Fe(CN)_6](BPDS)_{0.5} \cdot 4H_2O$	metamagnet	T_N = 3.3 K, B_c = 0.12 T (2 K)	pseudo 2D	35
$[Ni(1,1\text{-dmen})_2]_2[Fe(CN)_6](BPDS)_{0.5}$	ferromagnet	T_C = 10.7 K	squares Fe_4Ni_4	
$[Ni(1,1\text{-dmen})_2]_2[Fe(CN)_6](BPDS)_{0.5} \cdot 2H_2O$	metamagnet	T_N = 4 K, B_c = 0.4 T (2 K)		
$[Ni(L4)_2]_3[Fe(CN)_6]_2 \cdot 2H_2O$	ferromagnet	T_C = 14 K, B_c = 0.23 T (2 K)	2D rectangles Fe_6Ni_6	36
$[Ni(trans\text{-}(1S,2S)\text{-chxn})_2]_3[Fe(CN)_6]_2 \cdot 2H_2O$	ferromagnet	T_C = 13.8 K, B_c = 0.17 T (2 K)	2D	37
$[Ni(trans\text{-}(1R,2R)\text{-chxn})_2]_3[Fe(CN)_6]_2 \cdot 2H_2O$	ferromagnet	T_C = 13.8 K, B_c = 0.17 T (2 K)	rectangles Fe_6Ni_6	
$[Ni(1,1\text{-dmen})_2]_2[Fe(CN)_6]PhBSO_3 \cdot 5H_2O$	ferromagnet	T_C = 8.8 K, B_c = 0.015 T (2 K)	2D	38
$[Ni(1,1\text{-dmen})_2]_2[Fe(CN)_6]TolSO_3 \cdot 6H_2O$	ferromagnet	T_C = 9.5 K	squares Fe_4Ni_4	
$[Ni(dipn)]_3[Fe(CN)_6]_2 \cdot 7H_2O$	ferromagnet	T_C = 7.8 K, B_c = 0.0056 T (2 K)	3D	39
$[Ni(rac\text{-CTH})]_3[Fe(CN)_6]_2$	ferromagnet	T_C = 3 K, B_c = 0.0025 T (2 K)	1D $\{Fe_2Ni_2\}_{square}$-Ni subunits	40
$[Ni(trans\text{-}(1S,2S)\text{-chxn})_2]_3[Fe(CN)_6]_2 \cdot 2H_2O$	ferromagnet	T_C = 13.8 K, B_c = 0.17 T (2 K)	2D	41

dx.doi.org/10.1021/ic201358c |*Inorg. Chem.* 2011, 50, 9153–9163

Table 1. Continued

compound	type of magnetic ordering	critical parameters	structural motif	ref
$[Ni(trans\text{-}(1R,2R)\text{-chxn})_2]_3[Fe(CN)_6]_2\cdot 2H_2O$	ferromagnet	T_C = 13.8 K, B_c = 0.17 T (2 K)	rectangles Fe_6Ni_6	
$[Ni(L5)]_3[Fe(CN)_6]_2\cdot 2H_2O$	metamagnet	T_N = 5.2 K, B_c = 0.35 T (2 K)	3D	42
$Ni(cis\text{-}(1R,2S)\text{-chxn})_2]_3[Fe(CN)_6]_2\cdot 2H_2O$	ferromagnet	T_C = 11 K, B_c = 0.04 T (2 K)	2D rectangles Fe_6Ni_6	43
$Cs[Ni(L6)][Fe(CN)_6]_2\cdot 3H_2O$	metamagnet	T_N = 3.4 K	3D	44
$[Ni(dipn)]_2[Ni(dipn)(H_2O)][Fe(CN)_6]_2\cdot 11H_2O$	ferromagnet	T_C = 8.5 K, B_c = 0.035 T (2 K)	3D	45
$[Ni(en)_2]_3[Fe(CN)_6]_2\cdot 3H_2O$ (**1**)	metamagnet	T_N = 13 K, B_c = 1.1 T (2 K)	1D rope-ladder chain	this work
$[Ni(en)_2]_3[Fe(CN)_6]_2\cdot 2H_2O$ (**2**)	metamagnet	T_N = 13 K, B_c = 1.1 T (2 K)	1D rope-ladder chain	this work
$[Ni(en)_2]_3[Fe(CN)_6]_2$ (**3**)	metamagnet	T_N = 8.4 K, B_c = 0.35 T (2 K)	1D rope-ladder chain	this work

[a] Abbreviations: pn =1,2-diaminopropane; tren = tris(2-aminoethyl)amine; 1,1-dmen = 1,l-dimethylethylenediamine; bpm = bis(1-pyrazolyl)methane; cyclam = 1,4,8,11-tetraazacyclotetradecane; tn = trimethylenediamine; $BPDS^{2-}$ = biphenyl-4,4′-disulfonate; *trans*-chxn = *trans*-cyclohexane-1,2-diamine; *rac*-CTH = *rac*-5,7,7,12,14,14-hexamethyl-1,4,8,11-tetraazacyclotetradecane; L1 = 3,10-dimethyl-1,3,5,8,10,12-hexaazacyclotetradecane; L2 = 3,10-diethyl-1,3,5,8,10,12-hexaazacyclotetradecane; L3 = 3,10-dihydroxyethyl-1,3,6,8,10,12-hexaazacyclotetradecane; L4 = 1,2-diaminocyclohexane; L5 = *N*,*N*′-bis(3-aminopropyl)ethylenediamine; L6 = 2,4-diamino-1,3,5-triazin-6-yl-{3-(1,3,5,8,12-pentaazacyclotetradecane)}.

$K_3[Fe(CN)_6]$ in water it behaved as a paramagnet.[10] These discrepancies in its magnetic behavior were attributed to formation of quasi-two- and three-dimensional domains. It should be emphasized that only the susceptibility measurements were discussed by the cited authors; no more sophisticated magnetometry (magnetic hysteresis, zero-field-cooled or field-cooled magnetization) was reported, even though data from such experiments provide vital insights into the nature of a material's magnetic ordering. The controversial interpretation of the magnetic behavior of $\{[Ni(en)_2]_3[Fe(CN)_6]_2\cdot 2H_2O\}_n$ is all the more surprising considering that this compound has opened avenues to miscellaneous molecular magnets based on Ni(II) complex cations and the hexacyanoferrate(III) anion (see Table 1).

Prompted by the reported inconsistency in the magnetism of this first Ni−$Fe(CN)_6$-based molecular magnet and the understanding that crystal water molecules change the magnetic properties of cyanido-bridged molecular magnets,[11] we synthesized the following coordination polymers: $\{[Ni(en)_2]_3[Fe(CN)_6]_2\cdot 3H_2O\}_n$ (**1**), $\{[Ni(en)_2]_3[Fe(CN)_6]_2\cdot 2H_2O\}_n$ (**2**), and $\{[Ni(en)_2]_3[Fe(CN)_6]_2\}_n$ (**3**). The compounds were chemically and structurally characterized by elemental analysis, infrared spectroscopy, thermal analysis (TG/DTA), and single-crystal X-ray analysis. The metamagnetic behavior was established for all reported compounds, and by concurrent analyzing of magnetic and ^{57}Fe in-field Mössbauer spectroscopy data, the thorough magnetic phase diagrams were constructed. It was found that the number of crystal water molecules has a major effect on the Néel temperature, critical field, and magnetic hardness of compounds **1**−**3** in the ferromagnetic state.

EXPERIMENTAL SECTION

Materials and Methods. All of the starting chemicals were of analytical reagent grade and used as received. The $[Ni(en)_3]Cl_2\cdot 2H_2O$ precursor was prepared according to the literature procedure.[12] Elemental analysis (C, H, N) was performed on a FLASH 2000 CHNS Analyzer (ThermoFisher Scientific). Thermogravimetric (TG) and differential thermal analyses (DTA) were performed using a thermal analyzer Exstar TG/DTA 6200 (Seiko Instruments Inc.) in dynamic air conditions (100 mL/min) between room temperature (~20 °C) and 600 °C (gradient 2.5 °C/min). The infrared spectrum of the complex was recorded on a ThermoNicolet NEXUS 670 FT-IR spectrometer using the ATR technique on the diamond plate in the range of 400−4000 cm^{-1}. The transmission ^{57}Fe Mössbauer spectra were collected using a Mössbauer spectrometer in a constant acceleration mode with a $^{57}Co(Rh)$ source, and all presented data are relative to natural α-iron foil. Mössbauer spectroscopy measurements below room temperature and in-field experiments were carried out using a Spectromag system (Oxford Instruments). The magnetic properties were measured on polycrystalline powdered samples using a MPMS XL-7 Quantum Design SQUID magnetometer. Experimental data were corrected for the diamagnetism of the constituent atoms by using Pascals' constants and for the diamagnetism of the sample holder.

$\{[Ni(en)_2]_3[Fe(CN)_6]_2\cdot 3H_2O\}_n$ (1). Compound **1** was prepared by reacting 0.208 g (0.6 mmol) of $[Ni(en)_3]Cl_2\cdot 2H_2O$ in 100 mL of H_2O with 0.132 g (0.4 mmol) of $K_3[Fe(CN)_6]$ in 100 mL of H_2O. The solution was left to stand for 1 week, over which time period microcrystals of **1** formed. These were separated on a sintered funnel, washed with water, ethanol, and methanol, and dried in air. Yield: 60%. Anal. Calcd for $C_{24}H_{54}N_{24}O_3Fe_2Ni_3$: C, 28.41; H, 5.36; N, 33.13. Found: C, 28.45; H, 5.63; N, 33.02. IR (cm^{-1}): 3535 (w), 3432 (w), 3342 (s), 3286 (s), 3170 (w), 2963 (w), 2892 (w), 2152 (w), 2127 (s), 2109 (s), 1588 (s), 1459 (w), 1327 (w), 1275 (w), 1012 (s), 998 (m), 969 (m), 665 (m), 518 (s), 497 (s).

$\{[Ni(en)_2]_3[Fe(CN)_6]_2\cdot 2H_2O\}_n$ (2). Compound **2** was prepared by drying compound **1** at 65 °C for 2 h and cooling it in a desiccator. Anal. Calcd for $C_{24}H_{52}N_{24}O_2Fe_2Ni_3$: C, 28.92; H, 5.26; N, 33.73. Found: C, 28.45; H, 5.38; N, 33.41. IR (cm^{-1}): 3529 (w), 3433 (w), 3341 (s), 3287 (s), 3170 (w), 2963 (w), 2891 (w), 2152 (w), 2124 (s), 2109 (s), 1588 (s), 1457 (w), 1325 (w), 1274 (w), 1012 (s), 995 (s), 968 (m), 667 (m), 518 (s), 497 (s).

$\{[Ni(en)_2]_3[Fe(CN)_6]_2\}_n$ (3). Compound **3** was prepared by heating a sample of compound **1** in the oven at 140 °C for 2 h. It was then cooled in a desiccator and immediately subjected to elemental and X-ray analyses and studied by infrared and Mössbauer spectroscopies. The sample for magnetic measurement was prepared by heating a sample of **1** directly in the SQUID magnetometer at T = 400 K for 3 h and flushing the sample space with helium gas to remove water vapor. Anal. Calcd for $C_{24}H_{48}Fe_2N_{24}Ni_3$: C, 30.01; H, 5.04; N, 35.00. Found: C, 30.03; H, 5.06; N, 35.28. IR (cm^{-1}): 3380 (w), 3363

dx.doi.org/10.1021/ic201358c |*Inorg. Chem.* 2011, 50, 9153–9163

(m), 3334 (s), 3308 (s), 3280 (s), 3268 (s), 3168(m), 2958 (w), 2912 (w), 2893 (w), 2148 (w), 2128 (s), 2115 (s), 2104 (m), 1593 (s), 1461 (w), 1326 (w), 1280 (w), 1003 (s), 960 (m), 685 (m), 644 (m), 625 (m), 515 (s), 497 (s).

General Crystallographic Details. X-ray measurement on selected crystals of **1** and **3** was performed on an Oxford Diffraction Xcalibur™ equipped with a Sapphire2 CCD detector using Mo Kα radiation at 120 K. The CrysAlis program package (version 1.171.32.11, Oxford Diffraction) was used for data collection and reduction.[13] The molecular structures were solved by direct methods SHELX-97, and all non-hydrogen atoms were refined anisotropically on F^2 using the full-matrix least-squares procedure in SHELXS-97 with weight $w = 1/[\sigma^2(F_o)^2 + (0.047P)^2 + 3.122P]$, where $P = (F_o^2 + 2F_c^2)/3.37$.[14] All H atoms of **1** and **3** were found in differential maps of electron density, and their parameters were refined using the riding model with C−H distances of 0.950 (CH), and 0.990 (CH2) Å, respectively, and with $U_{iso}(H) = 1.2U_{eq}(C)$. The figures of the X-ray structures were processed using the Diamond software package.[15]

Crystal Data for 1. $C_{24}H_{54}Fe_2N_{24}Ni_3O_3$, $M = 1014.74$, $T = 120(2)$ K, black prism, 0.25 × 0.20 × 0.10 mm^3, triclinic, space group P-1, $a = 7.41714(19)$ Å, $b = 9.6389(2)$ Å, $c = 15.9662(4)$ Å, $\alpha = 74.928(2)°$, $\beta = 88.339(2)°$, $\gamma = 73.568(2)°$, $V = 1055.96(4)$ Å^3, $Z = 1$, $D_c = 1.596$ g/cm^3, $F_{000} = 526$, 10 162 reflections collected, 3732 unique ($R_{int} = 0.0171$), GooF = 1.067, $R_1 = 0.0200$, $wR_2 = 0.0508$, R indices calculated with $I > 2\sigma(I)$.

Crystal Data for 3. $C_{24}H_{48}Fe_2N_{24}Ni_3$, $M = 960.69$, $T = 120(2)$ K, black prism, 0.18 × 0.15 × 0.12 mm^3, triclinic, space group P-1, $a = 7.4441(5)$ Å, $b = 9.5528(6)$ Å, $c = 14.4550(8)$ Å, $\alpha = 78.584(5)°$, $\beta = 77.080(5)°$, $\gamma = 79.211(5)°$, $V = 971.02(10)$ Å^3, $Z = 1$, $D_c = 1.643$ g/cm^3, $F_{000} = 496$, 8890 reflections collected, 3401 unique ($R_{int} = 0.0436$), GooF = 0.938, $R_1 = 0.0467$, $wR_2 = 0.1099$, R indices calculated with $I > 2\sigma(I)$.

Theoretical Calculations Details for 1. The paramagnetic part of the temperature-dependent magnetization of **1** in the range from 25 to 300 K was analyzed using the finite-size closed chain approach according to the spin Hamiltonian in eq 2 (see also Scheme S1, Supporting Information). Such a high number of interacting spins results in a large interaction matrix which cannot be efficiently diagonalized. Using the spin-coupled basis set labeled as $|\alpha SM\rangle$ together with irreducible tensor operators technique,[16] where α stands for the intermediate quantum numbers denoting the coupling path, and assuming that all g factors are equal ($g_{Fe} = g_{Ni} = g$) enables us to factorize the zero-field states according to the final spin S. The largest dimension of the submatrix is 38 351 for $S = 2$ (Table S1, Supporting Information). Consequently, the energy levels in nonzero magnetic field are calculated as $\varepsilon_i(\alpha SM) = \varepsilon_{0,k}(\alpha S) + \mu_B g B M_S$. Furthermore, the spin-coupled basis set can be further factorized according to the irreducible representation of the C_{2v} symmetry point group. The numerically efficient route to use this so-called spin permutational symmetry (SPS) approach[17] demands the coupling scheme, which is left invariant under the symmetry operations of the point group. This condition is fulfilled for $\mathbf{S}_{A1} = \mathbf{S}_1 + \mathbf{S}_3$, $\mathbf{S}_{A2} = \mathbf{S}_4 + \mathbf{S}_5$, $\mathbf{S}_{A3} = \mathbf{S}_6 + \mathbf{S}_8$, $\mathbf{S}_{A4} = \mathbf{S}_9 + \mathbf{S}_{10}$, $\mathbf{S}_{A5} = \mathbf{S}_{11} + \mathbf{S}_{13}$, $\mathbf{S}_{A6} = \mathbf{S}_{14} + \mathbf{S}_{15}$, $\mathbf{S}_{B1} = \mathbf{S}_2 + \mathbf{S}_{A1}$, $\mathbf{S}_{B2} = \mathbf{S}_7 + \mathbf{S}_{A3}$, $\mathbf{S}_{B3} = \mathbf{S}_{12} + \mathbf{S}_{A5}$, $\mathbf{S}_{B4} = \mathbf{S}_{A2} + \mathbf{S}_{A4}$, $\mathbf{S}_{C1} = \mathbf{S}_{B1} + \mathbf{S}_{B2}$, $\mathbf{S}_{C2} = \mathbf{S}_{B3} + \mathbf{S}_{B4}$, $\mathbf{S}_D = \mathbf{S}_{C1} + \mathbf{S}_{C2}$, and $\mathbf{S} = \mathbf{S}_D + \mathbf{S}_{A6}$. The dimensions of the submatrices are listed in Table S1 (Supporting Information). Now, the largest matrix has the dimension of 19 236 for $S = 2$, $\Gamma = A_1$ and calculation of the whole energy spectrum is much faster. Having the energy levels labeled as $\varepsilon_i(\alpha SM,\Gamma_j) = \varepsilon_{0,k}(\alpha S,\Gamma_j) + \mu_B g B M$, the molar magnetization can be easily calculated as

$$M_{mol} = N_A \mu_B g \frac{\sum_i M_S \exp[-\varepsilon_i(\alpha SM,\Gamma_j)/kT]}{\sum_i \exp[-\varepsilon_i(\alpha SM,\Gamma_j)/kT]}$$

RESULTS AND DISCUSSION

Compound $\{[Ni(en)_2]_3[Fe(CN)_6]_2\cdot 3H_2O\}_n$ (**1**) was prepared by slow crystallization from an aqueous solution of $[Ni(en)_3]^{2+}$ and $[Fe(CN)_6]^{3-}$ as described in the Experimental Section. The resulting black crystals were analyzed by elemental analysis, infrared spectroscopy, TG/DTA, and single-crystal X-ray analyses, and all of the above-mentioned physical methods confirmed formation of **1**. TG/DTA analysis showed two steps of dehydration, see Figure S1 (Supporting Information). In the first step, within temperature interval $t \approx 60-70$ °C, one molecule of water is eliminated (weight loss found/calcd 1.9%/1.8%). The second dehydration step, corresponding to loss of two water molecules, starts above 100 °C and ends around 140 °C (weight loss found/calcd 3.5%/3.6%). The dehydrated compound is stable up to 200 °C. Above this temperature, decomposition occurs, accompanied by two sharp exoeffects at 275 and 300 °C. The final product is believed to be a mixture of NiO and $NiFe_2O_4$ in a molar ratio of 2:1 (weight residue found/calcd 37.2%/37.8%). On the basis of TG/DTA analysis of **1**, the next compound $\{[Ni(en)_2]_3[Fe(CN)_6]_2\cdot 2H_2O\}_n$ (**2**) was prepared by partial dehydration at 65 °C. The black crystals of **2** were analyzed in the same manner as for **1**. Alternatively, compound **2** can be prepared by drying compound **1** in a desiccator over concentrated H_2SO_4 or P_2O_5, as previously reported.[10] This compound is slightly hygroscopic and reforms the trihydrate compound **1** if exposed to humid air. Finally, the last compound $\{[Ni(en)_2]_3[Fe(CN)_6]_2\}_n$ (**3**) was prepared by complete dehydration of **1** at 140 °C; all physical analyses of this compound were performed immediately after cooling the sample in a desiccator.

Infrared spectroscopy of **1**−**3** corroborated the presence of the ethylendiamine ligand as indicated by the observation of ν(N−H), ν(C−H), and $\delta(NH_2)$ vibrations in the 3400−3200, 2970−2890, and 1593−1588 cm^{-1} regions as well as ν(C−C), ν(C−N), and $\rho_w(NH_2)$ vibrations in the 1015−960 cm^{-1} region and ring deformation vibrations in the 520−490 cm^{-1} region. The broad $\rho_r(NH_2)$ vibration found around 665 cm^{-1} in the spectra of **1** and **2** was split into three vibrations in the 625−685 cm^{-1} region in the case of **3**.[18] The ν(CN) vibrations of the terminal cyanido ligands were observed between 2155 and 2145 cm^{-1}; the vibrations of the bridging cyanido groups occurred in the 2130−2100 cm^{-1} region.[19] This region contained three major ν(CN) vibrations in the spectra of compound **3** but only two major vibrations in those of **1** and **2**. The crystal water ν(O−H) vibrations occurred at 3540−3430 cm^{-1} in the spectra of **1** and **2** but were absent in the spectrum of **3**, confirming successful dehydration. In summary, FTIR spectroscopy confirmed the similarity of the hydrated complexes **1** and **2** and the differences between these complexes and the dehydrated complex **3**.

The X-ray analyses were performed for compounds **1** and **3**, as the X-ray structure of **2** is already known.[9] The asymmetric units with labeling schemes and selected bond lengths and angles are in the Supporting Information (Figures S2−S3, Tables S2−S3). The coordination polymeric system $\{[Ni(en)_2]_3[Fe(CN)_6]_2\cdot xH_2O\}_n$ is composed of one-dimensional molecular rope-ladder chains, in which the ladders' backbones are formed by *zig-zagged* alternating chains of the *cis*-$[Ni(en)_2]^{2+}$ and $[Fe(CN)_6]^{3-}$ units and the *trans*-$[Ni(en)_2]^{2+}$ cations are connected to the $[Fe(CN)_6]^{3-}$ anions, forming the ladders' "rungs" (see Figure 1). The disorder of ethylenediamine ligands of *trans*-$[Ni(en)_2]^{2+}$ ions in **1** is

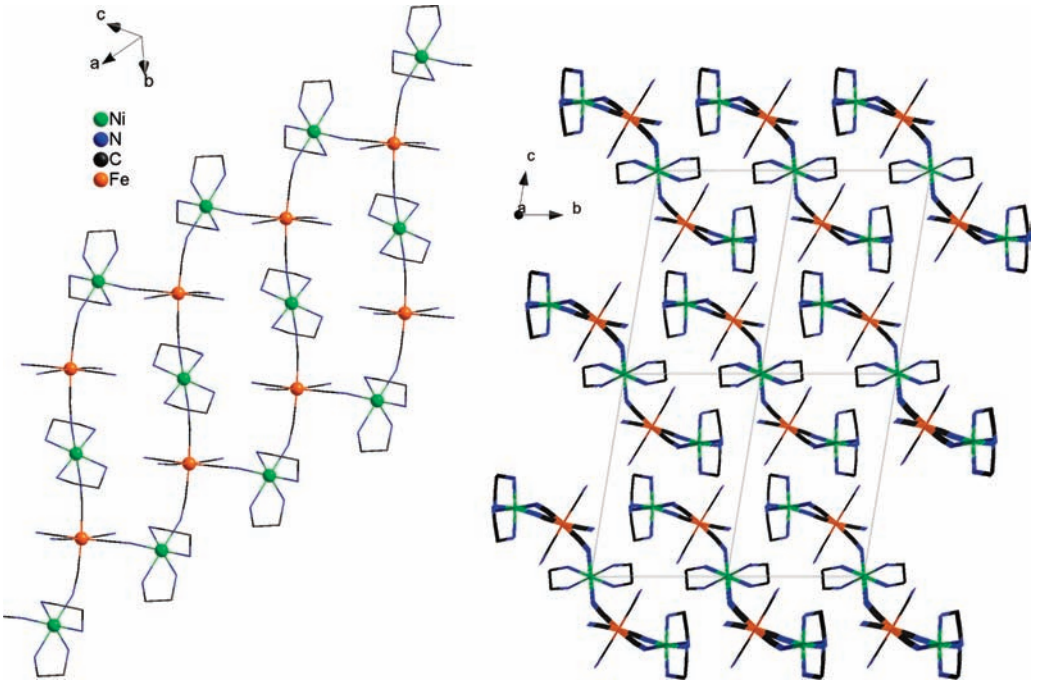

Figure 1. Part of the crystal structure of **3**, showing its rope-ladder chain structure (left) and chain packing (right); hydrogen atoms omitted for clarity.

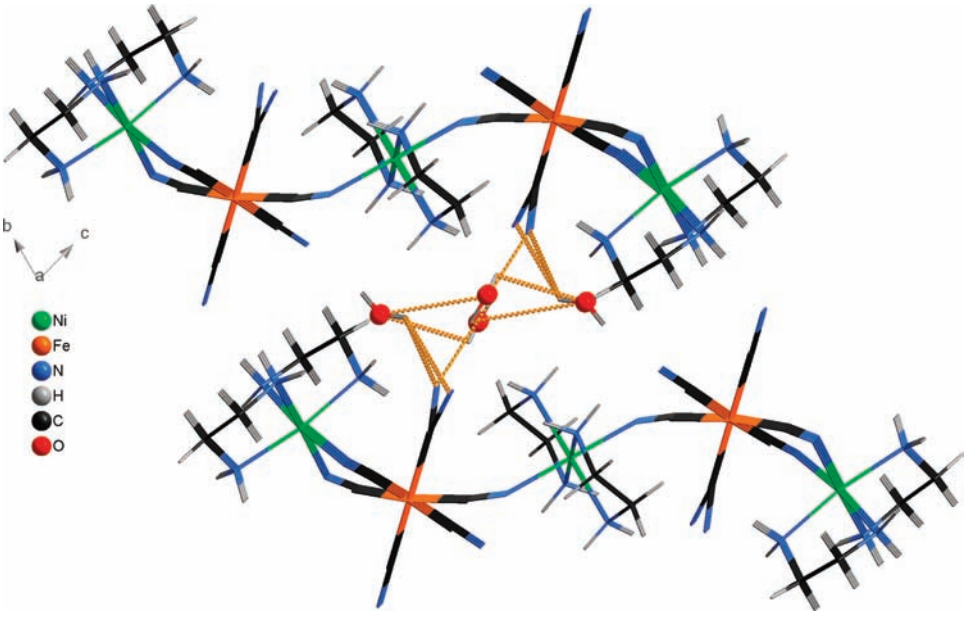

Figure 2. Part of the X-ray structure of **1** showing formation of the hydrogen-bond network among crystal water molecules and nitrogens of cyanido ligands between two different rope-ladder chains.

depicted in Figure S4 (Supporting Information). Upon total dehydration of **1**, topotactic transformation was observed, resulting in compound **3**. The primary rope-ladder chain-like crystal structure is preserved in **3**, accompanied by an 8% decrease of the unit cell volume and more compressed packing of the ladders. To visualize these structural differences, the packing of the individual ladders and crystal water molecules is depicted in Figure S5A (Supporting Information). The presence of three crystal water molecules in **1** results in formation of interchain hydrogen bonding of the O−H···O and O−H···N types occurring via the cyanido ligands (see Figure 2, Table S4 in the Supporting Information). As a consequence of the loss of one crystal water molecule in **2**, only the O−H···N interchain hydrogen bonds are observed. Thus, the interchain interactions are partially weakened (see Figure S5B and Table S4 in the Supporting Information). Both types of H bonds are completely missing in **3**, and only the interchain hydrogen bonding of the N−H···N type between the ethylenediamine ligand and the terminal cyano ligand is observed. These N−H···N interactions are very similar in compounds **1**−**3** (see Table S4 and Figure S5C,

dx.doi.org/10.1021/ic201358c |*Inorg. Chem.* 2011, 50, 9153–9163

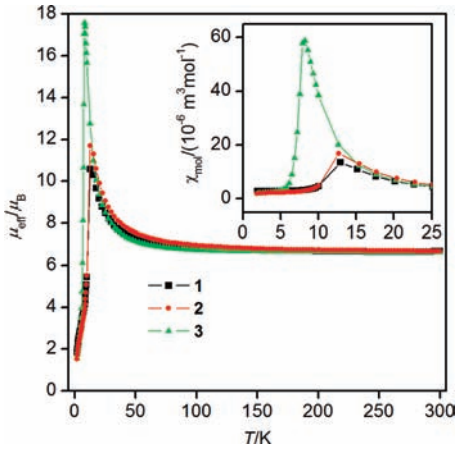

Figure 3. Comparison of the temperature-dependent magnetic data measured at $B = 0.1$ T for compounds **1**−**3**: effective magnetic moment and molar susceptibility (inset).

Supporting Information). Evidently, the differences in the magnetic properties of studied coordination polymers are mainly driven by the O−H···O and O−H···N hydrogen bonding while the role of N−H···N interactions seem to be considerably less important.

MAGNETIC STUDY

The temperature dependence of the effective magnetic moment of $\{[Ni(en)_2]_3[Fe(CN)_6]_2\cdot xH_2O\}_n$ (**1**−**3**), calculated from the mean susceptibility measured at $B = 0.1$ T, is shown in Figure 3. The effective magnetic moment of **1** and **2** is 6.67 μ_B at room temperature and gradually increases as the temperature is reduced; at temperatures below 50 K, a rapid increase in μ_{eff} is observed, peaking at ∼12 K, due to ferromagnetic interactions between the Ni(II) and the Fe(II) atoms within the rope-ladder chain. As the temperature is lowered still further, an abrupt decrease in μ_{eff} is observed; this is attributed to formation of interchain interactions that induce antiferromagnetic ordering. Compound **3** behaves similarly, but its maximum effective magnetic moment was found at 8 K and its maximum molar susceptibility was four times higher than that of compounds **1** and **2**, indicating that ferromagnetic exchange predominates in this compound. Theoretical analyses of the paramagnetic behavior based on the modified Curie−Weiss law

$$\chi_{mol} = \frac{N_A\mu_0\mu_B^2[3S_{Ni}(S_{Ni}+1)+2S_{Fe}(S_{Fe}+1)+]}{3k}\frac{g^2}{T-\Theta} \quad (1)$$

was used to fit the inverse susceptibilities of **1**−**3** above 30 K. As a result, the g factors and Weiss constants were extracted as follows: $g = 2.39$ and $\Theta = +8.8$ K (**1**), $g = 2.39$ and $\Theta = +11.7$ K (**2**), and $g = 2.39$ and $\Theta = +6.5$ K (**3**).

We also attempted to analyze the paramagnetic part of the molar susceptibility for **1** in order to estimate the value of the isotropic exchange between Ni(II) and Fe(III) cations mediated by the cyanido ligands. However, there is no theoretical formula for the susceptibility of an infinite one-dimensional rope-ladder chain with alternating spins $S_A = 1/2$ and $S_B = 1$. Therefore, the finite-size chain Heisenberg spin Hamiltonian has been postulated based on the crystal structure of **1**, according to Scheme S1 (Supporting Information), as

$$\hat{H} = -J\begin{pmatrix} S_1\cdot S_4 + S_4\cdot S_6 + S_6\cdot S_9 + S_9\cdot S_{11} + S_{11}\cdot S_{14} + S_{14}\cdot S_1 + \\ S_3\cdot S_5 + S_5\cdot S_8 + S_8\cdot S_{10} + S_{10}\cdot S_{13} + S_{13}\cdot S_{15} + S_{15}\cdot S_3 + \\ S_1\cdot S_2 + S_2\cdot S_3 + S_6\cdot S_7 + S_7\cdot S_8 + S_{11}\cdot S_{12} + S_{12}\cdot S_{13} \end{pmatrix} + \mu_B\sum_{i=1}^{15}\mathbf{B}\cdot\mathbf{g}_i\cdot\mathbf{S}_i \quad (2)$$

where J stands for the isotropic exchange between Ni(II) and Fe(III) centers. The exchange coupling of (Fe_6Ni_9) centers generates $N = (2S_{Fe}+1)^6(2S_{Ni}+1)^9 = 2^6 3^9 = 1\,259\,712$ magnetic states. Such a large interaction matrix was efficiently diagonalized using the irreducible tensor operators and spin permutational symmetry of the spin Hamiltonian as described in the Experimental Section. Finally, the molar magnetization in the temperature range from 30 to 300 K, in which the compound behaves as a paramagnet, was fitted, generating the following set of parameters: $J = +12.0$ cm^{-1}, $g = 2.31$, and $\chi_{TIP} = 13.7$ m^3 mol^{-1} (Figure S6, Supporting Information). A similar ferromagnetic exchange J value of 8.6 cm^{-1} has been observed in complexes such as $[Ni(tmphen)_2]_3[Fe(CN)_6]_2\cdot 14H_2O$ (tmphen = 3,4,7,8-tetramethyl-1,10-phenanthroline).[20]

To identify the nature of the sudden drops in the magnetic susceptibility and effective magnetic moments of compounds **1**−**3** at very low temperature, we conducted a thorough magnetic investigation and constructed magnetic phase diagrams (see Figure 4). For all three compounds, we observed exceptional field-induced transitions from the antiferromagnetic through the ferromagnetic to the paramagnetic phase, showing them to be molecular metamagnets. The magnetic properties of the compounds are discussed in detail in the following paragraphs.

For $\{[Ni(en)_2]_3[Fe(CN)_6]_2\cdot 3H_2O\}_n$ (**1**), the isothermal magnetic hysteresis loops measured in the range from 2 to 12 K show an abrupt increase in their magnetization under magnetic fields below ∼1.1 T, which is indicative of metamagnetic behavior.[21] Moreover, they indicate weak magnetic hysteresis at magnetic fields above ∼1.1 T, consistent with a transition from an antiferromagnetic to a ferromagnetic state (see Figure 5 and Figure S7, Supporting Information). The critical magnetic fields observed at a range of temperatures extracted from turn-points of the virgin magnetization curves (M_{mol} vs B) are plotted (as squares) in the magnetic phase diagram in Figure 4. The limiting critical magnetic field ($T \rightarrow 0$ K) is estimated as $B_c = 1.1$ T, indicating that the magnitude of the antiferromagnetic interaction among the 1D chains is approximately 0.74 K (0.51 cm^{-1}). The observed B_c is higher than previously reported values for any nickel(II)−hexacyanoferrate(III) metamagnets, see Table 1. In addition, field-cooled magnetization curves measured from 0.002 to 7 T demonstrate the compound's magnetic transitions to the antiferromagnetic state below 1.1 T and ferromagnetic states above B_c (see Figure 6). We extracted the dependence of the critical temperature on the magnetic field (see the magnetic phase diagram for **1** in Figure 4) by analyzing the zero-field-cooled (ZFC) and field-cooled (FC) magnetization curves.

Corresponding data obtained from analysis of $\{[Ni(en)_2]_3[Fe(CN)_6]_2\cdot 2H_2O\}_n$ (**2**) indicates that its magnetic behavior has an almost identical temperature dependence to that of **1** (see Figure 3), and the magnetic properties of its ordered phase are likely to be very similar. The critical magnetic field for the transition from the antiferromagnetic to the ferromagnetic phase, $B_c \approx 1.1$ T, was the same as that for **1**, as evidenced by the

dx.doi.org/10.1021/ic201358c |*Inorg. Chem.* 2011, 50, 9153–9163

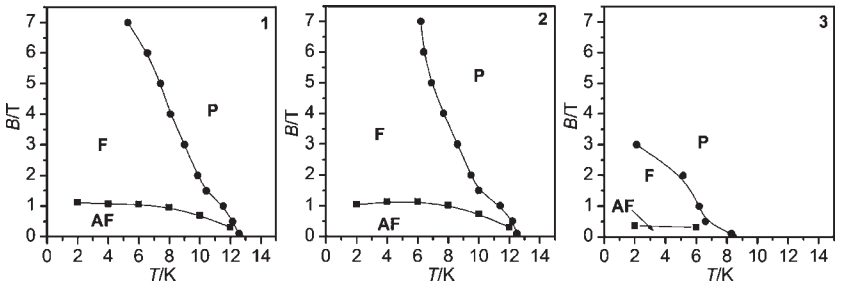

Figure 4. Magnetic phase diagrams for compounds **1**−**3**. Squares show the critical field derived from M_{mol} vs B data acquired at the indicated temperatures; circles show the critical temperature derived from ZFC/FC curves (M_{mol} vs T) under the indicated magnetic fields: F, ferromagnetic phase; AF, antiferromagnetic phase; P, paramagnetic phase. The lines connecting the points on the diagrams are visual guides only and should not be overinterpreted.

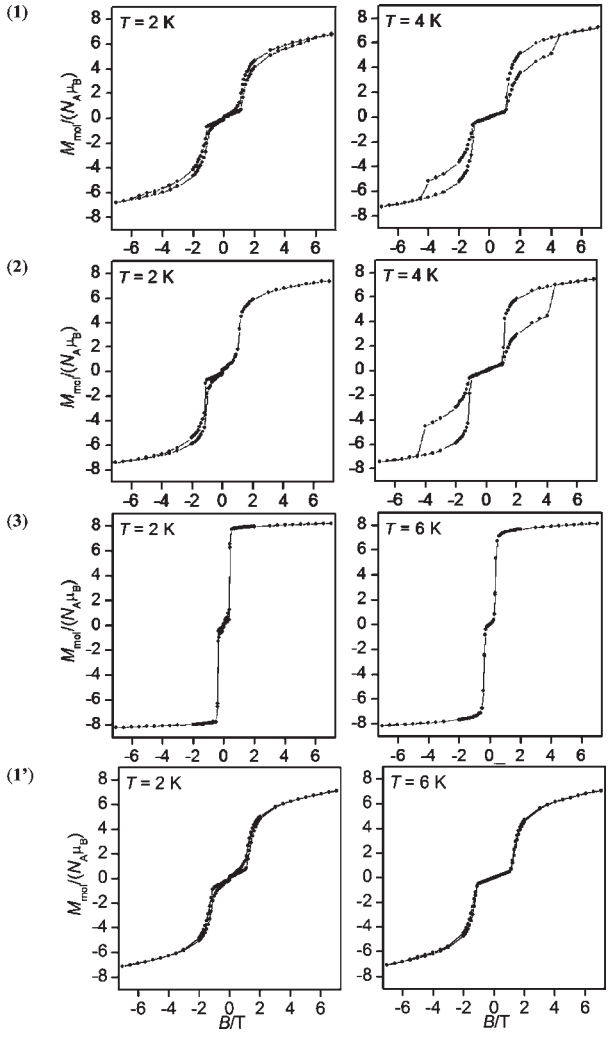

Figure 5. Magnetic hysteresis loops for compounds **1**−**3** and **1**′ recorded at the temperatures indicated.

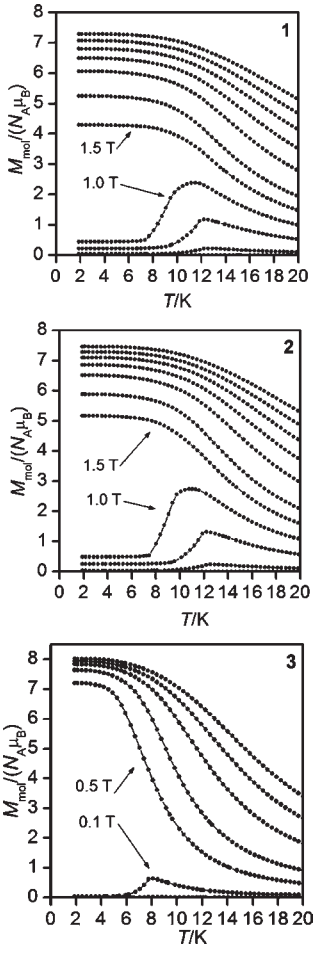

Figure 6. Field-cooled magnetization measurements of **1**−**3** for different magnetic fields (0.0002, 0.1, 0.5, 1, 1.5, 2, 3, 4, 5, 6, and 7 T) (**1** and **2**) and (0.0002, 0.1, 0.5, 1, 1.5, 2, 3, and 4 T) (**3**). The arrows show different behavior of FC curves for transitions to either the antiferromagnetic or the ferromagnetic state.

magnetic hysteresis loop measurements, performed under the same conditions as for **1** (see Figure 5 and Figure S8, Supporting Information). However, the loss of one molecule of the crystal water led to a dramatic increase in the magnetic hardness, manifested by an increase in the width of the magnetic hysteresis. The hysteresis loop opens below 10 K, with the maximum coercivity value found at T = 4 K, which is a typical behavior expected for ferromagnetic compounds. By combining the ZFC/FC results with hysteresis loop measurements, we also derived a magnetic phase diagram for compound **2** (see Figure 4). Surprisingly, on lowering the temperature to T = 2 K, we observed that the coercivity fell to almost zero for both **1** and **2**, indicating that their magnetic behavior may be more complex below 2 K.

dx.doi.org/10.1021/ic201358c |*Inorg. Chem.* 2011, 50, 9153–9163

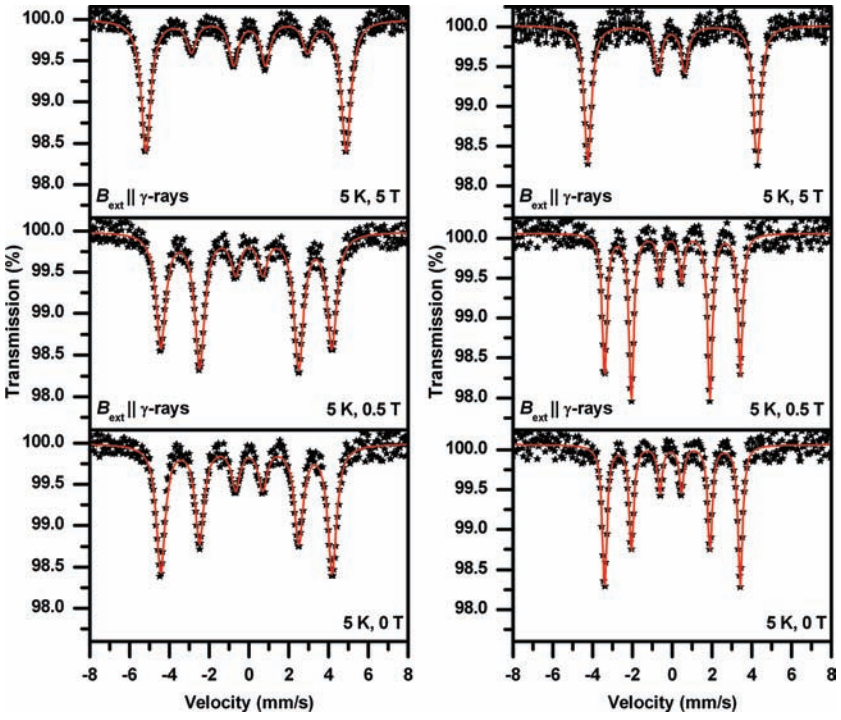

Figure 7. In-field Mössbauer spectra measured at T = 5 K for **2** (left) and **3** (right). The lines represent the fits with parameters in Table 2.

The last compound, $\{[Ni(en)_2]_3[Fe(CN)_6]_2\}_n$ (**3**), was prepared by direct dehydration of **1** in a SQUID magnetometer at 400 K, which resulted in formation of an anhydrous compound according to the acquired TG/DTA curves. Direct treatment in the magnetometer was used to prevent secondary hydration due to contact of the sample with air. The magnetic behavior of **3** differs strongly from that of **1** and **2**. Its maximum effective magnetic moment is much higher (17.6 μ_B) and occurs at a lower temperature (T = 8 K) than that of **1** (see Figure 3). It displayed typical metamagnetic responses in the isothermal magnetization measurements (see Figure 5), yielding an S-shaped curve. However, three main differences with respect to **1** were observed: (a) its critical field is reduced to B_c = 0.35 T, (b) there is no hysteresis in the ferromagnetic phase, and (c) its magnetization is sharply saturated after the transition from the antiferromagnetic state. In addition, the ZFC/FC magnetization curves indicated that a paramagnetic-to-ferromagnetic transition occurred in the magnetic field range of 0.35−3 T, but no differences between the ZFC and FC magnetization curves were observed on increasing the magnetic field, indicating the absence of a magnetic phase transition (see Figure 6 and Figure S9, Supporting Information). A magnetic phase diagram for **3,** constructed using the above-mentioned data, indicates that antiferro−ferro−paramagnetic-state transitions (i.e., AF−F−P-state transition) can be achieved below ∼6 K, simply by increasing the magnetic field intensity (see Figure 4). We also studied the effect of rehydration by leaving a sample of **3** in air for 1 week and repeating the magnetic hysteresis measurements. The resulting sample (**1′**) behaved almost identically to the original compound **1**, as clearly shown by the hysteresis loops obtained for the compounds (see Figure 5). To conclude, we report molecular systems offering all three (AF−F−P) magnetic regimes, which can be controlled both *chemically* (by varying the number of the crystal water molecules) and *physically* (by varying the temperature and magnetic field).

Table 2. Hyperfine Parameters of 2 and 3, Derived from Mössbauer Spectra, Measured at a Temperature of 5 K and under Various Inductions of an Applied Magnetic Field[a]

sample	T (K)	B_{ext} (T)	$\delta \pm 0.01$ (mm/s)	$\Delta E_Q \pm 0.01$ (mm/s)	$B_{hf} \pm 0.3$ (T)	$B_{eff} \pm 0.3$ (T)	$\Gamma \pm 0.01$ (mm/s)
2	5	0.0	−0.03	−0.13	27.8		0.48
		0.5	−0.04	−0.14		28.2	0.49
		5.0	−0.04	−0.14		30.9	0.61
3	5	0.0	−0.03	0.09	21.2		0.32
		0.5	−0.03	0.08		21.5	0.33
		5.0	−0.03	0.06		26.3	0.43

[a] T is the temperature of measurement, B_{ext} is the induction of the external magnetic field, δ is the isomer shift, ΔE_Q is the quadrupole splitting, B_{hf} is the hyperfine magnetic field, B_{eff} is the effective magnetic hyperfine field (given by the vector sum of the hyperfine magnetic field B_{hf} and external magnetic field, i.e., $\boldsymbol{B}_{eff} = \boldsymbol{B}_{hf} + \boldsymbol{B}_{ext}$), and Γ is the line width.

Moreover, the crystal water molecules affect dramatically the qualitative nature of the compound's ferromagnetic state, including its magnetic hardness and saturation capacity.

■ MÖSSBAUER SPECTROSCOPY

To obtain deeper insights into the magnetic behavior of compounds **1**−**3**, we recorded Mössbauer spectra at room temperature with no external magnetic field and at 5 K in magnetic fields ranging from 0.5 to 5 T parallel to the gamma-ray direction. Representative low-temperature Mössbauer spectra of compounds **2** and **3** are depicted in Figure 7, and the hyperfine parameters derived from the corresponding spectra are summarized in Table 2. In contrast to the magnetization measurements, ^{57}Fe Mössbauer spectroscopy monitors the local physical and

dx.doi.org/10.1021/ic201358c |*Inorg. Chem.* 2011, 50, 9153–9163

chemical environment around the iron nucleus. At 300 K, the Mössbauer spectrum of compound **1** (see Figure S10, Supporting Information) contains a doublet component with a rather asymmetric profile. The doublet asymmetry arises probably from the texture within the investigated sample **1** and/or the Goldanskii–Karyagin effect.[46] The value of the isomer shift δ (ca. − 0.13 mm/s) is typical of Fe^{3+} ions in a low-spin state (i.e., $S = 1/2$), and the nonzero value of the quadrupole-splitting parameter ΔE_Q (ca. 0.64 mm/s) indicates that the surroundings of the probed iron nuclei are not spherically symmetric.[46] The particles of the studied samples were well crystallized, without significant structural defects (i.e., point or line crystal defects), as evidenced by the observation of sharp Mössbauer lines with narrow line widths. Since only the doublet is observed, compound **1** behaves in a paramagnetic manner, as expected and previously demonstrated by the magnetization measurements. The Mössbauer spectra of compounds **2** and **3** both contain a doublet component with very similar hyperfine parameters to **1** at 300 K (not shown).

As the temperature falls below ~13 and ~8 K, compounds **1** (or **2**) and **3** enter a magnetically ordered state, respectively. Since the magnetization measurements had shown that compounds **1** and **2** display almost identical magnetic behavior, we performed low-temperature and in-field Mössbauer analyses only for **2** and **3**. At 5 K with no applied magnetic field, the Mössbauer spectra of **2** and **3** exhibit a magnetically split component with the Mössbauer hyperfine parameters listed in Table 2. Note that dehydration of the studied metamagnetic compounds changes the distribution of the electronic charge around the Fe nuclei and reduces the strength of the internal magnetic field at these nuclei. Furthermore, the reduced value of the line width parameter for **3** indicates that it has a higher degree of crystallinity than **2**.

It is well known that if a magnetic material displaying antiferromagnetic behavior is exposed to an external magnetic field applied in the direction of γ-rays, the intensities of the second and fifth Mössbauer sextet lines generally remain unchanged or are slightly enhanced when the characteristic switching field of the material is overcome. In contrast, for magnetic materials of ferromagnetic and/or ferrimagnetic nature, the intensities of the second and fifth Mössbauer sextet lines decrease due to the orientation of the atomic magnetic moments toward the direction of the external magnetic field. If complete alignment of atomic magnetic moments with the material is reached, the second and fifth Mössbauer sextet lines completely vanish. However, similar phenomena can be observed if the external magnetic field is strong enough to induce magnetization within a sample of a paramagnetic compound, making it impossible in some cases to distinguish between a completely aligned ferromagnetic and a highly field-ordered paramagnetic compound.[47] In particular, when **2** and **3** are exposed to an external magnetic field (B_{ext}) of 0.5 T, applied parallel to the direction of propagation of γ-rays, we observe an increase in the intensity of the second and fifth lines ($A_{2,5}$) (see Figure 7). Since $A_{2,5}$ reflects the degree of alignment of Fe atomic moments to the direction of the external magnetic field, its enhancement implies that Fe atomic moments tend to orientate perpendicular to the direction of B_{ext}. This behavior is typical of ideal antiferromagnetic materials, for which a spin-reorientation phenomenon is observed if the external magnetic field overcomes a characteristic spin-reorientation field. On increasing the value of B_{ext}, a decrease in $A_{2,5}$ is observed, implying that the Fe atomic magnetic moments gradually align in the direction of B_{ext}; such behavior is typical in materials exhibiting a ferromagnetic and/or ferrimagnetic state. At B_{ext} values below 5 T, a nonzero value of $A_{2,5}$ is observed for **2** (see Figure 7), signifying that the Fe atomic moments are not completely aligned in the direction of B_{ext}. The incomplete alignment of the Fe atomic magnetic moments below 5 T is consistent with expectations, since the hysteresis loop, measured at 6 K, does not reach saturation below 5 T (see Figure S8, Supporting Information). However, under these conditions the Fe atomic moments of compound **3** align precisely with B_{ext}, as demonstrated by a zero value of $A_{2,5}$, at least within the experimental error of the Mössbauer technique (see Figure 7). This is not surprising as the hysteresis loop of **3**, measured at 6 K, shows a tendency toward saturation below 5 T (see Figure 5). In other words, an external magnetic field of 5 T is sufficient to align all Fe atomic moments within compound **3**. Thus, dehydration reduces the extent to which the atomic moments of Fe resist aligning toward an applied magnetic field, relative to that observed in otherwise-comparable hydrated samples. The in-field Mössbauer spectroscopy data together with the magnetization measurements discussed in detail above demonstrate that the investigated samples displayed three well-defined magnetic states: an ideal antiferromagnetic state, an ideal ferromagnetic state, and a perfectly ordered paramagnetic state. Evidently, the studied molecular systems do not exhibit any canting phenomena as commonly observed in inorganic network-based metamagnets.

CONCLUSIONS

In summary, the molecular ladder system $\{[Ni(en)_2]_3[Fe(CN)_6]_2 \cdot xH_2O\}_n$ opens avenues to a new class of molecular materials affording magnetic multistability with unique antiferro–ferro–paramagnetic field-induced transitions. In addition to spin crossover complexes and the common metamagnets exhibiting two distinct magnetic regimes depending on temperature and field, respectively, these three-phase metamagnets have potential uses in a wide range of applications due to their ability to readily shift between three principal magnetic states. The number of crystal water molecules enables the magnetic properties (including critical fields and temperatures, and magnetic hardness) of these three-phase metamagnets to be controlled. Of course, the potential applications of such compounds would be greatly expanded if systems with critical temperatures around room temperature could be developed. The effect of the alternation of the crystal solvents on magnetic properties in such molecular magnetic materials will the topic of our future studies.

ASSOCIATED CONTENT

Supporting Information. TG/DTA curves for **1**, additional figures and tables of the X-ray structures of **1** and **3**, extra figures of magnetic data for **1**–**3**, and room-temperature Mössbauer spectrum of **1**. This material is available free of charge via the Internet at http://pubs.acs.org.

AUTHOR INFORMATION

Corresponding Author

*E-mail: radovan.herchel@upol.cz (R.H.); radek.zboril@upol.cz (R.Z.).

ACKNOWLEDGMENT

This work was financially supported by the Operational Program Research and Development for Innovations–European

Social Fund (grant no. CZ.1.05/2.1.00/03.0058) and grants from the Ministry of Education of the Czech Republic (nos. 1M6198959201 and MSM6198959218), the Academy of Sciences of the Czech Republic (KAN115600801), and the Czech Science Foundation (P207/11/0841).

REFERENCES

(1) (a) Chappert, C.; Fert, A.; Van Dau, F. N. *Nat. Mater.* **2007**, *6*, 813–823. (b) Bogani, L.; Wernsdorfer, W. *Nat. Mater.* **2008**, *7*, 179–186. (c) Felser, C.; Fecher, G. H.; Balke, B. *Angew. Chem., Int. Ed.* **2007**, *46*, 668–699. (d) Wernsdorfer, W. *Nat. Nano* **2009**, *4*, 145–146.

(2) (a) In *Magnetism: A Supramolecular Function*; Kahn, O., Ed.; NATO ASI Ser. C484; Kluwer Academic: Dordrecht, 1996. (c) Miller, J. S.; Drillon, M. (Eds.) *Magnetism: Molecules to Materials II-V. Molecule-Based Materials*; Wiley-VCH: Weinheim, 2001−2005.

(3) (a) Gatteschi, D.; Caneschi, A.; Pardi, L.; Sessoli, R. *Science* **1994**, *265*, 1054. (b) Alivisatos, A. P.; Barbara, P. F.; Castleman, A. W.; Chang, J.; Dixon, D. A.; Klein, M. L.; McLendon, G. L.; Miller, J. S.; Ratner, M. A.; Rossky, P. J.; Stupp, S. I.; Thompson, M. E. *Adv. Mater.* **1998**, *10*, 1297–1336. (c) Kahn, O. *Acc. Chem. Res.* **2000**, *33*, 647–657.

(4) (a) Larionova, J.; Chavan, S. A.; Yakhmi, J. V.; Froystein, A. G.; Sletten, J.; Sourisseau, C.; Kahn, O. *Inorg. Chem.* **1997**, *36*, 6374–6381. (b) Kahn, O.; Larionova, J.; Yakhmi, J. V. *Chem.—Eur. J.* **1999**, *5*, 3443–3449.

(5) (a) Dunbar, K. R.; Heintz, R. A. *Prog. Inorg. Chem.* **1997**, *45*, 283–391. (b) Verdaguer, M.; Bleuzen, A.; Marvaud, V.; Vaissermann, J.; Seuleiman, M.; Desplanches, C.; Scuiller, A.; Train, C.; Garde, R.; Gelly, G.; Lomenech, C.; Rosenman, I.; Veillet, P.; Cartier, C.; Villain, F. *Coord. Chem. Rev.* **1999**, *190−192*, 1023–1047. (c) Ohba, M.; Okawa, H. *Coord. Chem. Rev.* **2000**, *198*, 313–328. (d) Černák, J.; Orendáč, M.; Potočňák, I.; Chomič, J.; Orendáčová, A.; Skoršepa, J.; Feher, A. *Coord. Chem. Rev.* **2002**, *224*, 51–66. (e) Przychodzeń, P.; Korzeniak, T.; Podgajny, R.; Sieklucka, B. *Coord. Chem. Rev.* **2006**, *250*, 2234–2260. (f) Rebilly, J. N.; Mallah, T. Synthesis of single-molecule magnets using metallocyanates. In *Single-Molecule Magnets and Related Phenomena*; Springer-Verlag: Berlin, 2006; Vol. 122, p 103. (g) Tanase, S.; Reedijk, J. *Coord. Chem. Rev.* **2006**, *250*, 2501–2510. (h) Shatruk, M.; Avendano, C.; Dunbar, K. R. *Prog. Inorg. Chem.* **2009**, *56*, 155–334.

(6) Ferlay, S.; Mallah, T.; Ouahes, R.; Veillet, P.; Verdaguer, M. *Nature* **1995**, *378*, 701–703.

(7) (a) Miyasaka, H.; Matsumoto, N.; Okawa, H.; Re, N.; Gallo, E.; Floriani, C. *J. Am. Chem. Soc.* **1996**, *118*, 981–994. (b) Miyasaka, H.; Matsumoto, N.; Re, N.; Gallo, E.; Floriani, C. *Inorg. Chem.* **1997**, *36*, 670–676. (c) Miyasaka, H.; Okawa, H.; Miyazaki, A.; Enoki, T. *J. Chem. Soc., Dalton Trans.* **1998**, 3991–3996. (d) Miyasaka, H.; Okawa, H.; Miyazaki, A.; Enoki, T. *Inorg. Chem.* **1998**, *37*, 4878–4883. (e) Kou, H. Z.; Liao, D. Z.; Cheng, P.; Jiang, Z. H.; Wang, G. L. *Acta Chim. Sin.* **1999**, *57*, 409–414. (f) Smith, J. A.; Galan-Mascaros, J. R.; Clerac, R.; Dunbar, K. R. *Chem. Commun.* **2000**, 1077–1078. (g) Bhattacharjee, A.; Miyazaki, Y.; Nakazawa, Y.; Koner, S.; Iijima, S.; Sorai, M. *Physica B* **2001**, *305*, 56–64. (h) Coronado, E.; Gimenez-Saiz, C.; Nuez, A.; Sanchez, V.; Romero, F. M. *Eur. J. Inorg. Chem.* **2003**, 4289–4293. (i) Figuerola, A.; Diaz, C.; Ribas, J.; Tangoulis, V.; Sangregorio, C.; Gatteschi, D.; Maestro, M.; Mahia, J. *Inorg. Chem.* **2003**, *42*, 5274–5281. (j) Miyasaka, H.; Ieda, H.; Matsumoto, N.; Sugiura, K.; Yamashita, M. *Inorg. Chem.* **2003**, *42*, 3509–3515. (k) Zhang, D. P.; Wang, H. L.; Chen, Y. T.; Ni, Z. H.; Tian, L. J.; Jiang, J. Z. *Inorg. Chem.* **2009**, *48*, 11215–11225.

(8) (a) Sato, O. *Acc. Chem. Res.* **2003**, *36*, 692–700. (b) Sato, O. *J. Photochem. Photobiol., C: Photochem. Rev.* **2004**, *5*, 203–223. (c) Ohkoshi, S.; Tokoro, H.; Hashimoto, K. *Coord. Chem. Rev.* **2005**, *249*, 1830–1840. (d) Maurin, I.; Chernyshov, D.; Varret, F.; Bleuzen, A.; Tokoro, H.; Hashimoto, K.; Ohkoshi, S. *Phys. Rev. B* **2009**, *79*, 064420–064429. (e) Lynch, M. S.; Cheng, M.; Van Kuiken, B. E.; Khalil, M. *J. Am. Chem. Soc.* **2011**, *133*, 5255–5262.

(9) Ohba, M.; Maruono, N.; Okawa, H.; Enoki, T.; Latour, J. M. *J. Am. Chem. Soc.* **1994**, *116*, 11566–11567.

(10) Ohba, M.; Fukita, N.; Okawa, H. *J. Chem. Soc., Dalton Trans.* **1997**, 1733–1737.

(11) (a) Kaneko, W.; Ohba, M.; Kitagawa, S. *J. Am. Chem. Soc.* **2007**, *129*, 13706–13712. (b) Milon, J.; Daniel, M.-C.; Kaiba, A.; Guionneau, P.; Brandès, S.; Sutter, J.-P. *J. Am. Chem. Soc.* **2007**, *129*, 13872–13878. (c) Yanai, N.; Kaneko, W.; Yoneda, K.; Ohba, M.; Kitagawa, S. *J. Am. Chem. Soc.* **2007**, *129*, 3496–3497. (d) Du, M.; Bu, X. H. *Prog. Chem.* **2009**, *21*, 2458–2464. (e) Sun, W.-W.; Tian, C.-Y.; Jing, X.-H.; Wang, Y.-Q.; Gao, E.-Q. *Chem. Commun.* **2009**, 4741–4743. (f) Yoshida, Y.; Inoue, K.; Kurmoo, M. *Inorg. Chem.* **2009**, *48*, 10726–10736. (g) Motokawa, N.; Matsunaga, S.; Takaishi, S.; Miyasaka, H.; Yamashita, M.; Dunbar, K. R. *J. Am. Chem. Soc.* **2010**, *132*, 11943–11951.

(12) State, H. M. *Inorg. Synth.* **1960**, *6*, 200–201.

(13) *CrysAlis CCD and CrysAlis RED*, Version 1.171.33.52; Oxford Diffraction Ltd.: England, 2009.

(14) Sheldrick, G. M. *Acta Crystallogr., Sect. A* **2008**, *64*, 112–122.

(15) Brandenburg, K. *DIAMOND, Release 3.2g*; Crystal Impact GbR: Bonn, Germany, 1997−2011.

(16) Boča, R. *Theoretical Foundations of Molecular Magnetism*; Elsevier: Amsterdam, 1999.

(17) Waldmann, O. *Phys. Rev. B* **2000**, *61*, 6138–6144.

(18) Bennet, A. M. A.; Foulds, G. A.; Thornton, D. A.; Watkins, G. M. *Spectrochim. Acta* **1990**, *46A*, 13–22.

(19) Nakamoto, K. *Infrared and Raman Spectra of Inorganic and Coordination Compounds Part B*, 6th ed.; Wiley: New York, 2009.

(20) Berlinguette, C. P.; Galan-Mascaros, J. R.; Dunbar, K. R. *Inorg. Chem.* **2003**, *42*, 3416–3422.

(21) Stryjewski, E.; Giordano, N. *Adv. Phys.* **1977**, *26*, 487–650.

(22) Ohba, M.; Okawa, H.; Ito, T.; Ohto, A. *Chem.Commun.* **1995**, 1545–1546.

(23) Fallah, M. S. E.; Rentschler, E.; Caneschi, A.; Sessoli, R.; Gatteschi, D. *Angew.Chem.,Int.Ed.* **1996**, *35*, 1947–1949.

(24) Ohba, M.; Okawa, H. *Mol. Cryst. Liq. Cryst.* **1996**, *286*, 101–108.

(25) Langenberg, K. V.; Batten, S. R.; Berry, K. J.; Hockless, R. D. C.; Moubaraki, B.; Murray, K. S. *Inorg. Chem.* **1997**, *36*, 5006–5015.

(26) Ohba, M.; Okawa, H.; Fukita, N.; Hashimoto, Y. *J. Am. Chem. Soc.* **1997**, *119*, 1011–1019.

(27) Kou, H. Z.; Gao, S.; Bu, W. M.; Liao, D. Z.; Ma, B. Q.; Jiang, Z. H.; Yan, S. P.; Fan, Y. G.; Wang, G. L. *J. Chem. Soc., Dalton Trans.* **1999**, 2477–2480.

(28) Colacio, E.; Dominguez-Vera, J. M.; Ghazi, M.; Kivekas, R.; Lloret, F.; Moreno, J. M.; Stoeckli-Evans, H. *Chem.Commun.* **1999**, 987–988.

(29) Kou, H.-Z.; Gao, S.; Ma, B.-Q.; Liao, D.-Z. *Chem.Commun.* **2000**, 1309–1310.

(30) Zhang, S.-W.; Fu, D.-G.; Sun, W.-Y.; Hu, Z.; Yu, K.-B.; Tang, W.-X. *Inorg. Chem.* **2000**, *39*, 1142–1146.

(31) Kou, H.-Z.; Bu, W.-M.; Gao, S.; Liao, D.-Z.; Jiang, Z.-H.; Yan, S.-P.; Fan, Y.-G.; Wang, G.-L. *J. Chem. Soc., Dalton Trans.* **2000**, 2996–3000.

(32) Tanase, S.; Ferbinteanu, M.; Andruh, M.; Mathoniere, C.; Strenger, I.; Rombaut, G. *Polyhedron* **2000**, *19*, 1967–1973.

(33) Van Langenberg, K.; Hockless, D. C. R.; Moubaraki, B.; Murray, K. S. *Synth. Met.* **2001**, *122*, 573–580.

(34) Shen, Z.; Zuo, J.-L.; Shi, F.-N.; Xu, Y.; Song, Y.; You, X.-Z.; Raj, S. S. S.; Fun, H.-K.; Zhou, Z.-Y.; Che, C.-M. *Transition Met.Chem.* **2001**, *26*, 345–350.

(35) Usuki, N.; Ohba, M.; Okawa, H. *Bull. Chem. Soc. Jpn.* **2002**, *75*, 1693–1698.

(36) Bellouard, F.; Clemente-Leon, M.; Coronado, E.; Galan-Mascaros, J. R.; Gomez-Garcia, C. J.; Romero, F.; Dunbar, K. R. *Eur. J. Inorg. Chem.* **2002**, 1603–1606.

(37) Coronado, E.; Gomez-Garcia, C. J.; Nuez, A.; Romero, F. M.; Rusanov, E.; Stoeckli-Evans, H. *Inorg. Chem.* **2002**, *41*, 4615–4617.

(38) Usuki, N.; Ohba, M.; Okawa, H. *Mol. Cryst. Liq. Cryst. Sci. Technol., Sect. A* **2002**, *376*, 59–64.

(39) Ohba, M.; Yamada, M.; Usuki, N.; Okawa, H. *Mol. Cryst. Liq. Cryst. Sci. Technol., Sect. A* **2002**, *379*, 241–246.
(40) Colacio, E.; Dominguez-Vera, J. M.; Lloret, F.; Rodriguez, A.; Stoeckli-Evans, H. *Inorg. Chem.* **2003**, *42*, 6962–6964.
(41) Coronado, E.; Gimenez-Saiz, C.; Martinez-Agudo, J. M.; Nuez, A.; Romero, F. M.; Stoeckli-Evans, H. *Polyhedron* **2003**, *22*, 2435–2440.
(42) Saha, M. K.; Moron, M. C.; Palacio, F.; Bernal, I. *Inorg. Chem.* **2005**, *44*, 1354–1361.
(43) Coronado, E.; Gomez-Garcia, C. J.; Nuez, A.; Romero, F. M.; Waerenborgh, J. C. *Chem. Mater.* **2006**, *18*, 2670–2681.
(44) Atanasov, M.; Comba, P.; Forster, S.; Linti, G.; Malcherek, T.; Miletich, R.; Prikhod'ko, A. I.; Wadepohl, H. *Inorg. Chem.* **2006**, *45*, 7722–7735.
(45) Yanai, N.; Kaneko, W.; Yoneda, K.; Ohba, M.; Kitagawa, S. *J. Am. Chem. Soc.* **2007**, *129*, 3496–3497.
(46) Greenwood, N. N.; Gibb, T. C. *Mössbauer Spectroscopy*; Chapman and Hall: London, 1971.
(47) Johnson, C. E. *J. Phys. D: Appl. Phys.* **1996**, *29*, 2266–2273.